ELSEVIER

Dynamics of Atmospheres and Oceans
33 (2001) 135–156

dynamics of atmospheres and oceans

www.elsevier.com/locate/dynatmoce

Symmetry properties of barotropic bottom-dissipated single-gyre systems in the inertial regime

Fulvio Crisciani [a], Tamay M. Özgökmen [b,*]

[a] *CNR, Instituto Talassografico di Trieste, Trieste, Italy*
[b] *Department of Meteorology and Physical Oceanography, Rosenstiel School of Marine and Atmospheric Science, University of Miami, 4600 Rickenbacker Causeway, Miami, FL 33149-1098, USA*

Accepted 8 May 2000

Abstract

Symmetry properties of steady solutions of the barotropic quasigeostrophic vorticity equation are explored using mirror reflections with respect to mid-basin longitude and latitude. The analysis is conducted by perturbing the fully inertial solution, the zeroth-order solution or the Fofonoff mode, by introducing forcing and dissipation as a first order correction. In the context of a classical square-basin and single-gyre circulation subject to bottom friction, it is shown numerically and analytically that the full solution can be approximated by the superposition of three components each having definite symmetry properties under longitude and latitude reflections: the north–south symmetric and antisymmetric components of the zeroth-order solution and the east–west antisymmetric component of the first-order correction. The flow patterns of the individual components are discussed.

Keywords: Inertial regime; Barotropic; Symmetry; Vorticiy equation

1. Introduction

The sequence of calculations produced in the pioneering work of Veronis (1966), that describes the evolution of the flow field of an idealized subtropical region for increasing nonlinearity with respect to bottom dissipation, is probably well engraved in the memory of every physical oceanographer. These experiments show, among other things, the gradual formation of the north–south asymmetry produced by the northward advection of vorticity and the tendency of the circulation patterns to loose progressively their east–west asymmetry until the disappearance for sufficiently high nonlinearity. The understanding of the evolution

* Corresponding author. Tel.: +1-305-361-4053; fax: +1-305-361-4696.
E-mail address: tozgokmen@rsmas.miami.edu (T.M. Özgökmen).

0377-0265/01/$ – see front matter
PII: S0377-0265(00)00055-5

of the streamline geometry pointed out by the experiments presupposes a distinction among three basic dynamical regimes that we call weakly nonlinear, intermediate and fully inertial. In the weakly nonlinear regime, the total solution can be expressed as the sum of the local terms (inertial+boundary layer contribution) and the dominant feature of the the streamlines, that is the westward intensification, can be deduced in two ways: by checking a posteriori its presence in each special solution or by resorting to general arguments such as Rossby wave dynamics (Pedlosky, 1965) or steady wind-driven flow energetics (Crisciani and Purini, 1997). We stress, however, that these last methods do not rely at all on the details of the forcing, being based only on the assumption of a viscosity dominated system. On the contrary, in the intermediate regime, as we shall see, the very nonlinearity that prevents local solutions, sheds light on the asymmetries of the gyre and only basic features of the forcing field are requested to explain the space structure of the solution within a framework of properly scaled equations of motion. This is the goal of the present paper. For completeness, we recall also that in the fully nonlinear regime, the interior velocity is so large that it makes unimportant the beta term in the vorticity equation, so that the solution comes from the balance between the bottom friction term and the forcing. If, as in Veronis' (1966) experiments, the forcing is invariant under the east–west exchange, then the east–west asymmetry disappears completely from this solution. In the intermediate regime, the interior velocity is much larger than the characteristic Sverdrup velocity but the beta term is still important. In this case, the center of the gyre tends to be in the northwestern area of the basin, thus stressing the northward displacement, typical of nonlinearity, and at the same time a weakening of the westward intensification.

Our aim is to relate these asymmetries to the dynamics of nonlinear subtropical gyres by means of the basic ingredients of the basin-scale wind-driven circulation. A hint on this subject has been given in an investigation on Niiler's (1966) solution of the basins-cale circulation problem. In fact, recently the analytical evaluation of the complete solution (Crisciani, 1998) exhibits, as a first-order correction, a cyclone–anticyclone couple aligned on a common latitude, with high pressure in the west and low pressure in the east. The superposition of this field to the zeroth-order correction, i.e. Fofonoff's (1954) mode with a northern circulation core, generates a weak intensification of the total northward current along the western boundary and a weakening of the total southern current along the eastern boundary. Thus, the intensification of Niiler's solution comes from the combined effect of the zeroth and first-order correction of the total solution. We wish to underline that the weak southward current of the interior, coming from the Sverdrup balance between the first-order correction and the wind-stress curl, does not expand, of necessity, as a couple cyclone–anticyclone in the whole basin. For instance, also a pure anticyclonic first-order correction, opportunely intensified on the west but consistent with the Sverdrup balance in the interior, could lead to a similar total solution after its superposition with Fofonoff's zeroth-order solution.

The idea in this study is to reconsider Niiler's model supplied with a forcing usually employed in single-gyre models and to investigate if the mechanism previously found in the special solution is preserved independently of adopted the forcing field. For this purpose, we solve numerically Niiler's model equations with two typical choices of the wind-stress curl and reconstruct, on the basis of the numerical output, the zeroth and first-order partial solutions.

The main result of this study is that the total solution is, up to the first-order correction, the sum of three components having definite symmetry properties under latitude and longitude reflections. We emphasize, however, that these symmetry properties appear to be valid for the particular, classical ocean model configuration, and the derivation of such properties for a class of basins and a class of wind forcings is a formidable task, which is not attempted here.

It is acknowledged by the authors that when compared to recent realistic numerical simulations, the specific results presented in this paper may not be directly related to aspects of the real ocean circulation. However, the solutions of the barotropic vorticity equation have been of interest to applied mathematics-oriented theoretical oceanographers for a long time. Furthermore, as we shall see also in this paper, this problem still offers considerable complexity and it is far from being completely solved analytically, despite of being one of the simplest equations employed to model ocean dynamics.

The paper is organized as follows: in Section 2, we introduce the model equations and define symmetric and antisymmetric components under mirror reflection transforms. We obtain numerical solutions for the zeroth and (approximate) first-order components and observe their symmetry properties in Section 3. In Section 4, we discuss the analytical arguments for the observed symmetry properties of the zeroth-order solutions, while those of the first-order solution are presented in Section 5. Features of a highly inertial subtropical gyre are discussed on the basis of these symmetry properties in Section 6. Finally, we summarize and conclude in Section 7.

2. Model equations

We recall the governing equations of the quasigeostrophic version of Niiler's model. Their derivations, with full details, can be found in Crisciani (1998). We underline once again that the key assumption is a flow field having a characteristic Sverdrup velocity much smaller than the interior velocity and denote by $\delta(\ll 1)$ their ratio. The nondimensional model equations are

$$\epsilon^2 J(\psi, \nabla^2\psi) + \frac{\partial \psi}{\partial x} = \delta(\underline{k} \cdot \underline{\nabla} \times \underline{\tau} - \epsilon \nabla^2\psi) \quad \forall \underline{x} \in D, \tag{1}$$

$$\psi = 0 \quad \forall \underline{x} \in \partial D \tag{2}$$

where $D = [0 \leq x \leq 1] \times [0 \leq y \leq 1]$ is the fluid domain and $\epsilon(\ll 1)$ is the nondimensional inertial boundary layer thickness. Eq. (1) includes the parameters δ and ϵ whose relative magnitude depends on the dynamical regime of interest. As, in the inertial regime, we can assume δ getting smaller and smaller, we must accordingly request a definite behavior to the equation itself in the limit for $\delta \to 0$. If $\epsilon \geq \delta$, δ and hence the whole rhs of Eq. (1) go to zero without influencing the lhs of the same equation. Therefore, the dominant vorticity equation turns out to be simply $J(\psi, \epsilon^2\nabla^2\psi + y) = 0$. On the contrary, if $\epsilon < \delta$, the dynamical balance between the rhs and the lhs of Eq. (1) is preserved whatever $\delta(\ll 1)$ may be. This is the regime we investigate in the following. The reason is that a solution, describing both the westward intensification and the northward displacement of the gyre,

is not consistent with an interior strictly zonal as that implied by every unforced balance. Substitution of the truncated expansion $\psi \approx \psi_0 + \delta\psi_1$ into Eqs. (1) and (2) gives, to zeroth and first-order in δ, respectively,

$$\epsilon^2 J(\psi_0, \nabla^2\psi_0) + \frac{\partial\psi_0}{\partial x} = 0 \quad \forall \underline{x} \in D, \tag{3}$$

$$\psi_0 = 0 \quad \forall \underline{x} \in \partial D \tag{4}$$

and

$$\epsilon^2[J(\psi_0, \nabla^2\psi_1) + J(\psi_1, \nabla^2\psi_0)] + \frac{\partial\psi_1}{\partial x} = \underline{k} \cdot \underline{\nabla} \times \underline{\tau} - \epsilon\,\nabla^2\psi_0 \quad \forall \underline{x} \in D, \tag{5}$$

$$\psi_1 = 0 \quad \forall \underline{x} \in \partial D. \tag{6}$$

The classical solution of Niiler and the numerical solutions of problems (1) and (2) that is described in the successive sections, point out two kinds of asymmetries in the geometry of the streamlines: one is related to the northward displacement of the center of the gyre while the second looks like a weak westward intensification. So, on the whole, the core of the gyre tends to be located in the north-western area of the basin.

To deal with the north–south asymmetry, it is useful to introduce the 'mirror reflection' transform of D into itself defined by

$$(x, y) \to (x, 1 - y) \tag{7}$$

and denote by a tilde every transformed quantity. For instance

$$\tilde{\psi}(x, y) = \psi(x, 1 - y) \tag{8}$$

and, in particular, the Jacobian and the Laplacian operators transform as

$$\tilde{J} = -J, \qquad \tilde{\nabla}^2 = \nabla^2. \tag{9}$$

Every field can be expressed as the sum of a symmetric part (s), that is invariant under transform (7), and an antisymmetric part (a) that simply changes sign under transform (7). For instance, with reference to Eq. (8), we write $\psi = (1/2)(\psi + \tilde{\psi}) + (1/2)(\psi - \tilde{\psi})$ and define $\psi^{(s)} = (1/2)(\psi + \tilde{\psi})$, $\psi^{(a)} = (1/2)(\psi - \tilde{\psi})$. Thus,

$$\psi = \psi^{(s)} + \psi^{(a)}. \tag{10}$$

Obviously, $\tilde{\psi}^{(s)} = \psi^{(s)}$ while $\tilde{\psi}^{(a)} = -\psi^{(a)}$. Similarly, the east–west asymmetry can be investigated with the aid of the transform given by

$$(x, y) \to (1 - x, y). \tag{11}$$

We use an overbar to state that

$$\overline{\psi}(x, y) = \psi(1 - x, y) \tag{12}$$

and, as in Eq. (9), we recall that

$$\overline{J} = -J, \qquad \overline{\nabla}^2 = \nabla^2. \tag{13}$$

We define $\psi_s = (1/2)(\psi + \overline{\psi})$, $\psi_a = (1/2)(\psi - \overline{\psi})$ so that

$$\psi = \psi_s + \psi_a. \tag{14}$$

As before, $\overline{\psi}_s = \psi_s$ while $\overline{\psi}_a = -\psi_a$. Moreover, hereafter we set

$$\underline{k} \cdot \underline{\nabla} \times \underline{\tau} = T_s(x, y) + T_a(x, y) \tag{15}$$

and postulate $T_s(x, y) \leq 0$, $T_a(x, y) \equiv 0$ in accordance with the common idealizations of the large-scale, subtropical wind forcing.

We end this section by noting that, whatever the antisymmetric functions $\chi^{(a)}$ and χ_a may be, we have

$$\int_D \chi^{(a)} \, d\underline{x} = 0 \quad \text{and} \quad \int_D \chi_a \, d\underline{x} = 0. \tag{16}$$

3. Numerical results

In order to observe the circulation patterns of the symmetric and antisymmetric components of a highly inertial subtropical gyre defined in Section 2, direct numerical solutions of Eq. (1) subject to boundary condition (2) are obtained in a rectangular domain. The prognostic version of Eq. (1) is integrated in time to a steady-state using a predictor–corrector type leapfrog method (Gazdag, 1976). The Jacobian operator $J(a, b) = a_x b_y - a_y b_x$ is computed using the formulation proposed by Arakawa (1966) that conserves kinetic energy and enstrophy, while accurately maintaining the property $J(a, b) = -J(b, a)$. The other terms are approximated by central differencing in space. The diagnostic equation for vorticity, $\zeta = \nabla^2 \psi$, is inverted to calculate the streamfunction using a fast Fourier transform solver (Swarztrauber, 1977).

The parameters for the numerical integrations are selected as follows. Since we are interested in a regime in which the interior velocity is much higher than the characteristic Sverdrup velocity, while there are still signs of westward intensification, the parameter δ is taken as 0.1 ($\ll 1$). The parameter ϵ, which is the nondimensional width of the inertial boundary layer, is related to δ through the relationship $\epsilon^2 \delta = U_S / \beta L^2$ (Crisciani, 1998), where U_S is the Sverdrup velocity, β is the planetary vorticity gradient and L is the horizontal length scale. Using typical values for these parameters, $U_S \approx 10^{-3}\,\mathrm{ms}^{-1}$, $\beta \approx 10^{-1}\,\mathrm{m}^{-1}\,\mathrm{s}^{-1}$ and $L \approx 10^6\,\mathrm{m}$, we take $\epsilon = 0.05\,(< \delta)$. The integrations are carried out with a numerical resolution of 101 grid points in each direction, such that inertial boundary layers are resolved (nearly identical solutions are obtained with 51 grid points in each direction as those presented below).

The first set of numerical experiments are conducted using a wind-stress curl dependent only on latitude: $T_s(y) = -\pi \sin(\pi y)$. The results are illustrated in Fig. 1. Fig. 1a and b show the steady-state solutions for the streamfunction and vorticity satisfying Eq. (1) for $\delta = 0.1$ and $\epsilon = 0.05$. In this parameter regime, the gyre center is located in the north-western area of the basin, indicating asymmetries in both the east–west and also north–south directions.

The symmetry properties of the full solution are explored by first analyzing those of the zeroth-order solution. The zeroth-order solution is approximated by reducing δ to 0.001

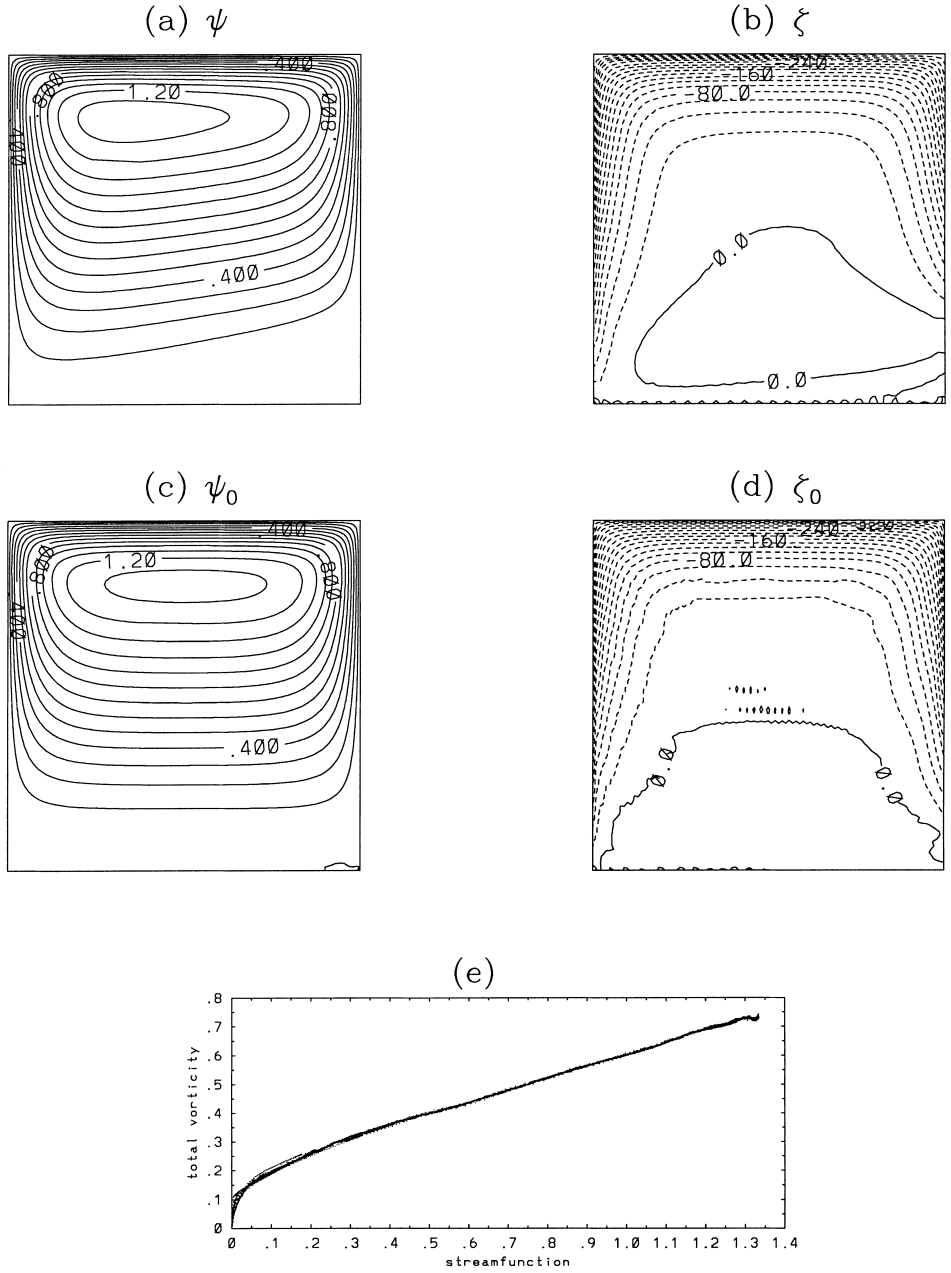

Fig. 1. Numerical experiments with the wind-stress curl $T_s(y) = -\pi \sin(\pi y)$; (a) steady-state streamfunction ψ (CI = 0.1) and (b) corresponding vorticity (CI = 20) for $\epsilon = 0.05$ and $\delta = 0.1$. Approximate zeroth-order solution (c) ψ_0 (CI = 0.1) and (d) corresponding relative vorticity (CI = 20) for $\epsilon = 0.05$ and $\delta = 0.001$. (e) The scatter plot of the total vorticity $\epsilon^2\nabla^2\psi_0 + y$ vs. ψ_0, (f) $\psi_0^{(s)}$ (CI = 0.05), (g) $\psi_0^{(a)}$ (CI = 0.05), (h) $\boldsymbol{D}$ (CI = 0.01), (i) $\boldsymbol{D}_s$ (CI = 0.01).

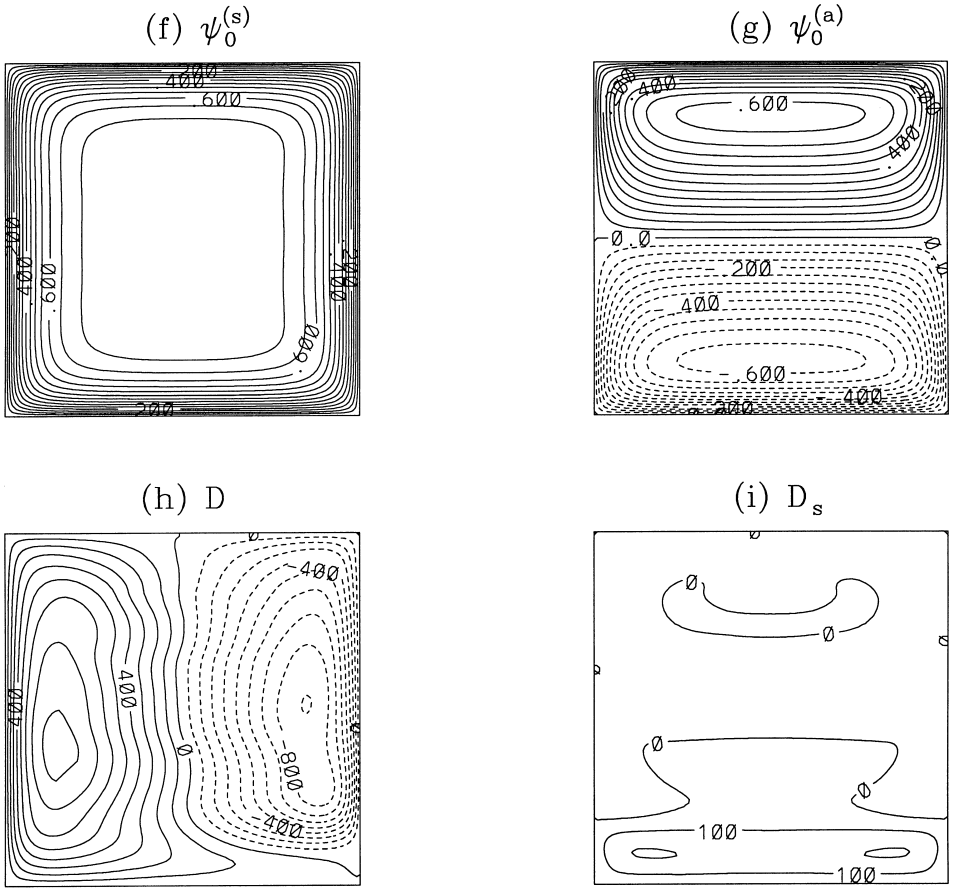

Fig. 1. (*Continued*).

(and keeping $\epsilon = 0.05$ as before) such that the rhs of Eq. (1) tends to 0 and Eq. (3) is approached numerically. The solutions are plotted in Fig. 1c and d. The gyre corresponding to the zeroth-order solution is symmetric in the east–west direction. We also show the scatter plot of the total vorticity $\epsilon^2\nabla^2\psi_0 + y$ versus ψ_0 in Fig. 1e, which demonstrates a nearly linear relationship with a positive slope. This functional relationship is of significant importance for the analytical derivations that are presented in the following sections.

In Fig. 1c, the center of the zeroth-order solution is displaced to the north leading to a north–south asymmetry. The symmetry properties of ψ_0 are explored from the numerical solution by plotting $\psi_0^{(s)}$ and $\psi_0^{(a)}$ in Fig. 1f and g, respectively. $\psi_0^{(s)}$ is an anticyclonic circulation following the boundaries and vanishing in the interior. The component $\psi_0^{(a)}$ represents an anticyclone in the northern half of the basin and a cyclone in the southern basin.

The first-order solution ψ_1 is not readily available from the full solution ψ (Fig. 1a) and the zeroth-order solution ψ_0 (Fig. 1c). Therefore, we construct an approximation to ψ_1 within an error of $O(\delta)$ by defining a residual streamfunction $\boldsymbol{D} = \psi - \psi_0 = \delta\psi_1 + O(\delta^2)$. The isolines of $\boldsymbol{D}$ are illustrated in Fig. 1h, which shows an anticyclone–cyclone couple, with high pressure in the west and low pressure in the east. This is consistent with the analytical evaluation of the first-order correction by Crisciani (1998). In spite of the qualitative resemblance between the numerical solution obtained in this paper and the analytical solution by Crisciani (1998), we stress the impossibility of following here the previous procedure to deduce the first-order correction and its symmetry properties. In fact, for this purpose, we need to know the details of the zeroth-order solution which corresponds, in the paper by Crisciani (1998), to the Fofonoff mode. We recall that this kind of zeroth-order solution was chosen a priori by Niiler (and his 'nonstandard' forcing was subsequently adapted), while in the present case, we have chosen a more conventional forcing and then computed (within a certain approximation) the zeroth-order solution. Because of this method, quite usual indeed, we do not have at our disposal any analytical form of the zeroth-order solution, and the boundary layer approach to calculate the first-order correction, as in Crisciani (1998), is no longer possible. Obviously, we could take into account, for instance, a linear approximation of the kind $F(\psi_0) = a\psi_0 + b$ by means of a best fit applied to the scatter plots in Figs. 1e and 2e, but we can easily think that the results would be as much similar to that obtained by Crisciani (1998) as dissimilar from the fields reported in Figs. 1h and 2h. The flow field in Fig. 1h is nearly antisymmetric under the transformation (11). This point is demonstrated more quantitatively by plotting the east–west symmetric components of $\boldsymbol{D}$, i.e. $\boldsymbol{D}_s = \delta\psi_{1s} + O(\delta^2)$, (Fig. 1i, the contour interval is equal to $\delta^2 = 0.01$). Aside from a small region along the southern boundary, where the second-order correction term may be important, this plot indicates that the east–west symmetric component of the first-order correction is zero. At this point, it is beneficial to relate this result to those obtained by Zimmerman and Maas (1989), who have investigated the symmetry properties of the solutions of the standard quasi-geostrophic vorticity equation on the beta-plane, for a bottom dissipated single fluid layer, from the point of view of the Green's function for forced circulation. Indeed, this function contains all symmetry properties of the full nonlinear vorticity equation. Due to the multipole character of the Green's function's relative vorticity field, it is possible to show, in particular, that 'the dynamics of the quadrupole governs the symmetry breaking around the dipole axis, being strongest for intermediate nonlinearity'. Actually, the cyclonic and anticyclonic centers are not perfectly symmetrically placed in Fig. 1h, and the trace of the quadrupole tilting predicted by Zimmerman and Maas (1989) in the almost free inertial limit, governed by Eq. (1), or by (7.15) of their paper, is apparent.

Numerical experiments are also performed with another wind-stress curl: $T_s(x, y) = -\pi \sin(\pi x) \sin(\pi y)$, which depends on both latitude and longitude (used also by Veronis, 1966). The parameter values for ϵ and δ are the same as those selected for the previous set of experiments (Fig. 1), the differences in the resulting circulation being due to changes in the wind forcing only. The results, illustrated in Fig. 2, are qualitatively the same as those shown in Fig. 1, with the exception of $\psi_0^{(s)}$, which exhibits anticyclonic loops (Fig. 2f). These loops are addressed in the following analytical arguments among with all the other properties observed in the numerical solutions. In general, the results shown in Fig. 2 appear

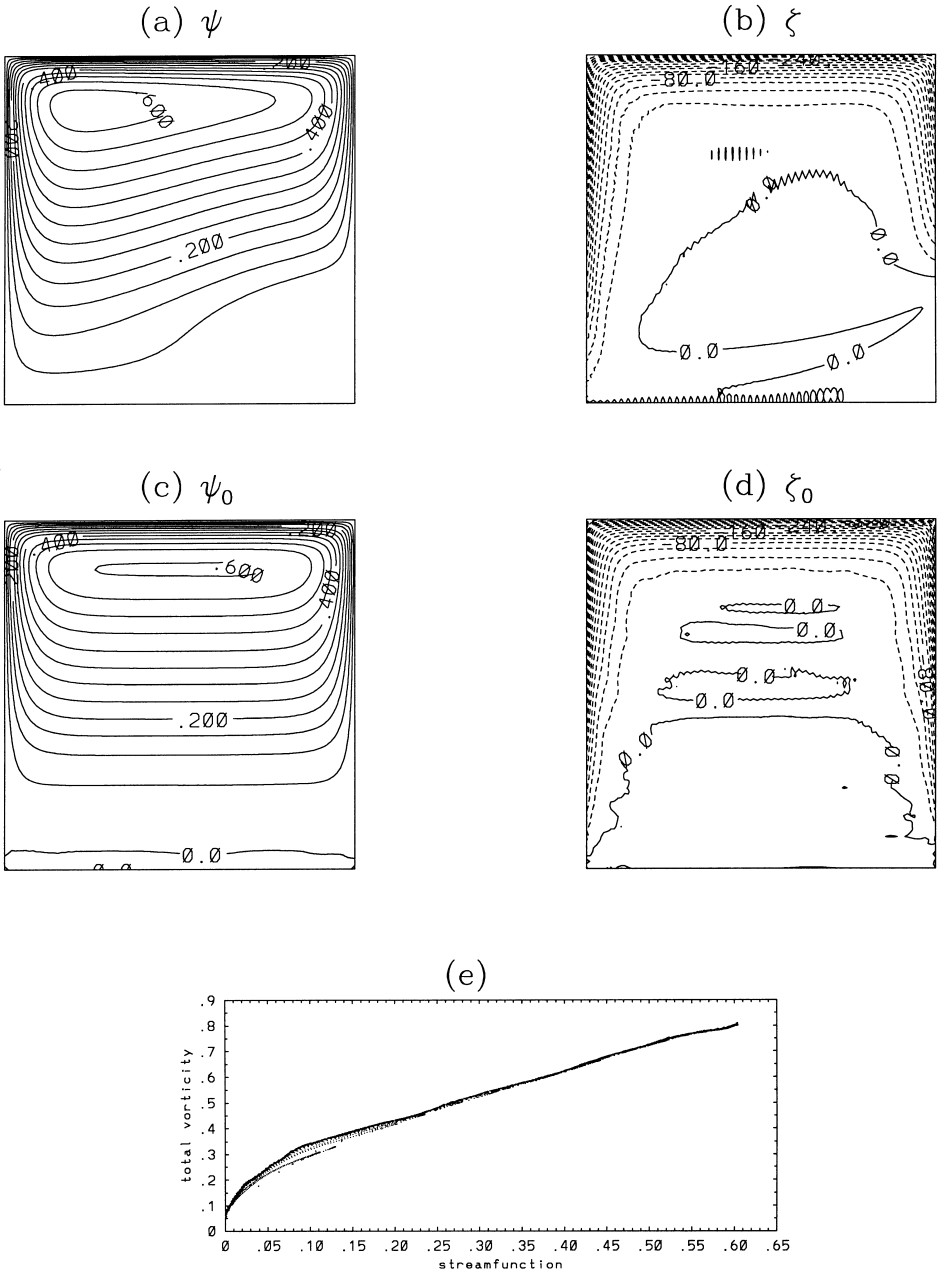

Fig. 2. Numerical experiments with the wind-stress curl $T_s(y) = -\pi \sin(\pi y) \sin(\pi x)$; (a) steady-state streamfunction ψ (CI = 0.05) and (b) corresponding relative vorticity (CI = 20) for $\epsilon = 0.05$ and $\delta = 0.1$. Approximate zeroth-order solution (c) ψ_0 (CI = 0.05) and (d) corresponding vorticity (CI = 20) for $\epsilon = 0.05$ and $\delta = 0.001$. (e) The scatter plot of the total vorticity $\epsilon^2 \nabla^2 \psi_0 + y$ vs. ψ_0, (f) $\psi_0^{(s)}$ (CI = 0.05), (g) $\psi_0^{(a)}$ (CI = 0.05), (h) $\boldsymbol{D}$ (CI = 0.01), (i) $\boldsymbol{D}_s$ (CI = 0.01).

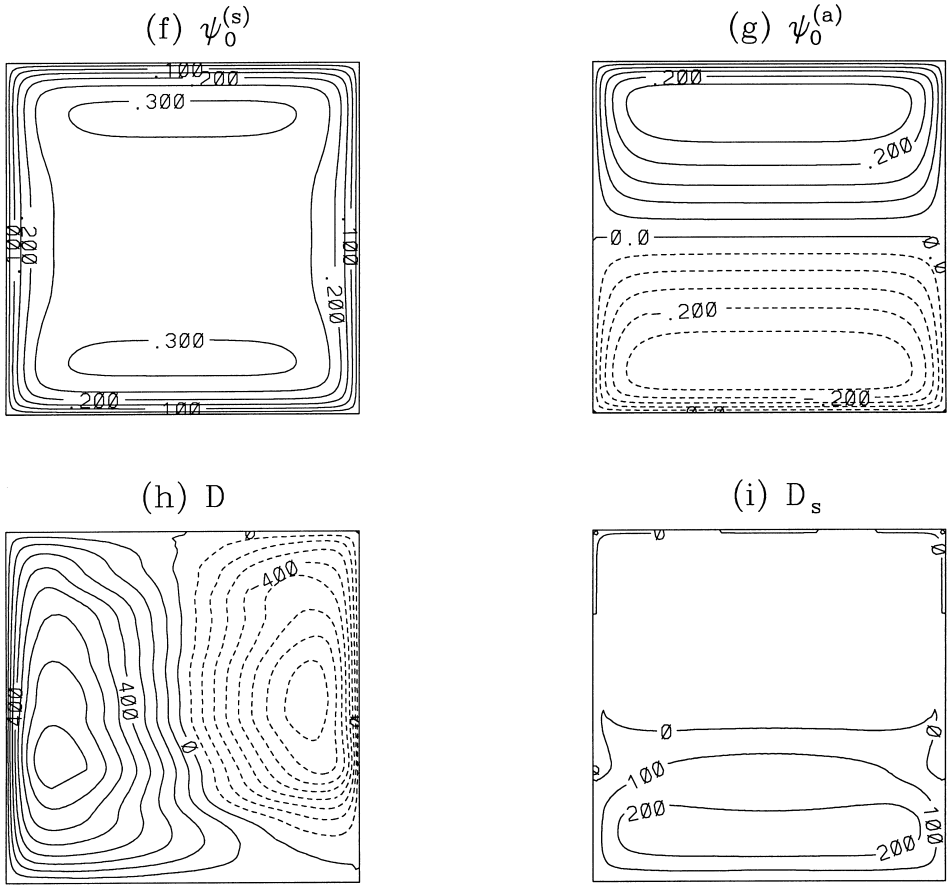

Fig. 2. (*Continued*).

to indicate that the symmetry properties are not greatly sensitive to the details of the wind forcing.

4. Symmetric and antisymmetric components of the zeroth-order solution

In order to explain the observed behavior of the symmetric and antisymmetric components of ψ_0 in the numerical solution, we start from the zeroth-order Eq. (3), which is equivalent to

$$\epsilon^2 \nabla^2 \psi_0 + y = F(\psi_0) \tag{17}$$

where $F(\psi_0)$ is a differentiable function of its argument. Although every differentiable $F(\psi_0)$ is able to satisfy Eq. (3), this function is actually related to the forcing through

Eq. (5). But, once the forcing is given, the determination of $F(\psi_0)$ is a very complex problem in general. Here, in accordance with Niiler's solution and the numerical solution described in the previous section (Figs. 1e and 2e), we take $F(\psi_0)$ unifunctional and

$$\frac{\partial F}{\partial \psi_0} > 0. \tag{18}$$

The inequality (18) is an important assumption which prevents the following analytical derivations from being a priori predictions about the nature of the flow components. We emphasize that nothing can be said about the sign of $\partial F/\partial \psi_0$ a priori. We base this assumption primarily on our numerical solutions, and also point out that no other assumption is made about the form of $F(\psi_0)$.

In the basin interior, due to the smallness of ϵ^2, the vorticity equation (17) becomes $y \approx F(\psi_0)$, so that $u_0 \approx -(\partial F^{-1}(y)/\partial y)$ and, because of Eq. (18), u_0 is westward there (< 0).

4.1. East–west symmetry

The inequality (18) allows us to show that,

$$\psi_0 = \psi_{0s}, \tag{19}$$

so ψ_0 is invariant under the mirror reflection (11). In fact, transform (11) applied to Eq. (17) gives

$$\epsilon^2 \nabla^2 \overline{\psi_0} + y = F(\overline{\psi_0}) \tag{20}$$

and subtracting Eq. (20) from Eq. (17), we have

$$\epsilon^2 \nabla^2(\psi_0 - \overline{\psi_0}) = F(\psi_0) - F(\overline{\psi_0}).$$

Hence,

$$\epsilon^2(\psi_0 - \overline{\psi_0})\nabla^2(\psi_0 - \overline{\psi_0}) = (\psi_0 - \overline{\psi_0})^2 \frac{F(\psi_0) - F(\overline{\psi_0})}{\psi_0 - \overline{\psi_0}},$$

that is to say

$$\begin{aligned} &\epsilon^2 \nabla \cdot [(\psi_0 - \overline{\psi_0})\nabla(\psi_0 - \overline{\psi_0})] - \epsilon^2 |\nabla(\psi_0 - \overline{\psi_0})|^2 \\ &\quad = (\psi_0 - \overline{\psi_0})^2 \frac{F(\psi_0) - F(\overline{\psi_0})}{\psi_0 - \overline{\psi_0}}. \end{aligned} \tag{21}$$

Integration of Eq. (21) on D gives

$$-\epsilon^2 \int_D |\nabla(\psi_0 - \overline{\psi_0})|^2 \, \mathrm{d}\underline{x} = \int_D (\psi_0 - \overline{\psi_0})^2 \frac{F(\psi_0) - F(\overline{\psi_0})}{\psi_0 - \overline{\psi_0}} \, \mathrm{d}\underline{x}. \tag{22}$$

The lhs of Eq. (22) is nonpositive while, due to Eq. (18), the rhs is nonnegative. Therefore, $\psi_0 = \overline{\psi_0}$ and Eq. (19) follows. This kind of invariance is consistent with the numerical results shown in Figs. 1c and 2c.

A useful integral balance between forcing and circulation follows from Eq. (5) that, by using Eqs. (15) and (17), can be written as

$$\epsilon^2 J(\psi_0, \nabla^2\psi_1) + J(\psi_1, F(\psi_0)) = T_s(\underline{x}) - \epsilon \nabla^2\psi_0. \tag{23}$$

In fact, if R is any region of the basin encircled by a (closed) streamline of ψ_0, then, since ψ_0 and $F(\psi_0)$ are constant along ∂R, integration of Eq. (23) on R gives

$$\int_R T_s \, \mathrm{d}\underline{x} = \epsilon \oint_{\partial R} \underline{u}_0 \cdot \mathrm{d}\underline{t} \tag{24}$$

where $\underline{u}_0 = \underline{k} \times \underline{\nabla}\psi_0$ is the zeroth-order geostrophic current and $\mathrm{d}\underline{t}$ is the infinitesimal line element tangent to ∂R. Eq. (24) will be repeatedly used.

4.2. North–south asymmetry

Zeroth-order solutions reported in Figs. 1c and 2c illustrate that the center of the gyre is displaced northward. To explain this observation using the physics of Niiler's model, we apply transform (8) and expansion (10) to Eq. (3) and obtain the following coupled equations for $\psi_0^{(s)}$ and $\psi_0^{(a)}$:

$$\epsilon^2[J(\psi_0^{(s)}, \nabla^2\psi_0^{(a)}) + J(\psi_0^{(a)}, \nabla^2\psi_0^{(s)})] + \frac{\partial\psi_0^{(s)}}{\partial x} = 0 \tag{25}$$

and

$$\epsilon^2[J(\psi_0^{(s)}, \nabla^2\psi_0^{(s)}) + J(\psi_0^{(a)}, \nabla^2\psi_0^{(a)})] + \frac{\partial\psi_0^{(a)}}{\partial x} = 0. \tag{26}$$

Because of the beta effect, Eq. (25) implies that $\psi_0^{(a)}$ cannot be identically vanishing. In fact $\psi_0^{(a)} = 0$ implies that $\psi_0^{(s)}$ is strictly zonal but, in this case, boundary condition (4) in turn implies $\psi_0^{(s)} = 0$ everywhere in the basin so, on the whole, $\psi_0 \equiv 0$. In the interior, using the main vorticity balance together with Eq. (10), we can write

$$\psi_0^{(s)} + \psi_0^{(a)} \approx F^{-1}(y). \tag{27}$$

Transform (8) applied to Eq. (25) yields

$$\psi_0^{(s)} - \psi_0^{(a)} \approx F^{-1}(1 - y) \tag{28}$$

and adding Eq. (27) to Eq. (28) gives $\psi_0^{(a)} \approx (1/2)[F^{-1}(y) - F^{-1}(1 - y)]$. In particular, $\psi_0^{(a)}(x, (1/2)) = 0$ in the interior and, because of the unifunctional structure of F and Eq. (18), the sole latitude where $\psi_0^{(a)}$ vanishes is just $y = 1/2$. Since the interior zonal current is westward, $\psi_0^{(a)}$ represents an anticyclone in the northern basin a cyclone in the southern basin. These arguments explain the patterns depicted in Figs. 1g and 2g.

Eq. (26) indicates a vanishing symmetric component, as it may be the case of some solutions of the fully inertial problems (3) and (4). However, this hypothesis is not consistent with Niiler's model. Indeed, if R coincides with D, Eqs. (16) and (24) yield

$$\int_D T_s(\underline{x})\,\mathrm{d}\underline{x} = \epsilon \int_D \nabla^2 \psi_0^{(s)}\,\mathrm{d}\underline{x} \tag{29}$$

where, in a subtropical gyre,

$$\int_D T_s(\underline{x})\,\mathrm{d}\underline{x} < 0. \tag{30}$$

Hence, Eqs. (29) and (30) prevent the solution $\psi_0^{(s)} \equiv 0$. On the contrary, in terms of the current $\underline{u}_0^{(s)} = ((-\partial\psi_0^{(s)}/\partial y), (\partial\psi_0^{(s)}/\partial x))$, Eqs. (29) and (30) imply

$$\oint_{\partial D} \underline{u}_0^{(s)} \cdot \mathrm{d}\underline{t} < 0. \tag{31}$$

The inequality (31) means an *anticyclonic circulation*, forced by the wind via Eq. (29) along the boundary, but it does not give us further details on the circulation close to the boundary itself. Two possible flows are reported in Figs. 1f and 2f. The anticyclonic loops in Fig. 2f are difficult to explain fully due to the coupled nature of Eqs. (25) and (26), but this issue can be partially addressed by recognizing that these loops overlap with the 'flat' region of $\psi_0^{(a)}$ (Fig. 2g). Consider Eq. (26) written as: $\epsilon^2 J(\psi_0^{(s)}, \nabla^2\psi_0^{(s)}) + J(\psi_0^{(a)}, \epsilon^2\nabla^2\psi_0^{(a)} + y) = 0$. Inside the strip marking the approximate latitudinal extent of the loops $\psi_0^{(a)} \approx \psi_0^{(a)}(x)$. So, in this region Eq. (26) becomes: $\epsilon^2 J(\psi_0^{(s)}, \nabla^2\psi_0^{(s)}) + (\partial/\partial x)\psi_0^{(a)} = 0$. This explains why, due to the intersection between the streamlines of $\psi_0^{(s)}$ and $\nabla^2\psi_0^{(s)}$ (not shown), the Jacobian $J(\psi_0^{(s)}, \nabla^2\psi_0^{(s)}) \neq 0$ inside the strips. Therefore, the anticyclonic loops in Fig. 2f are ultimately ascribed to the presence of a flat region encircled by a streamline of $\psi_0^{(a)}$ (Fig. 2g).

The damping factor ϵ in Eq. (29) requires a suitable intensification of the anticyclonic circulation in order to balance the O(1) contribution of the wind-stress curl on the rhs of Eq. (29). By using Eqs. (27) and (28) we have in the interior $\psi_0^{(s)} \approx (1/2)[F^{-1}(y) + F^{-1}(1-y)]$ and therefore: (i) trivially $(\partial\psi_0^{(s)}/\partial x) \equiv 0$, (ii) because of the linearity of $F(\psi_0)$ in the interior, also $F^{-1}(\psi_0)$ is linear in y and hence $F^{-1}(y) + F^{-1}(1-y)$ is constant, so that also $(-\partial\psi_0^{(s)}/\partial y) \equiv 0$. Thus, everywhere in the interior $\psi_0^{(s)} =$ constant, that is $\underline{u}_0^{(s)} \equiv 0$. Under these circumstances, Eq. (26) becomes $J(\psi_0^{(a)}, \epsilon^2\nabla^2\psi_0^{(a)} + y) = 0$. Fig. 1g indicates that the last equation is satisfied in the interior by a solution of the kind $\psi_0^{(a)} = \psi_0^{(a)}(y)$. More precisely, the linearity of $F^{-1}(y)$ implies $\psi_0^{(a)} \propto y - (1/2)$. The linear dependence of $\psi_0^{(a)}$ on latitude is also confirmed by the equal spacing of the isolines in the interior, as is evident in Figs. 1g and 2g. According to Eq. (26), outside the interior the evolution of total vorticity $\epsilon^2\nabla^2\psi_0^{(a)} + y$ is no longer inertial, but forced by $J(\psi_0^{(s)}, \nabla^2\psi_0^{(s)})$, so the amplitude of $T_s(\underline{x})$ controls not only that of $\psi_0^{(s)}$ through (24) but also that of $\psi_0^{(a)}$ through Eq. (26).

Hence, the sum of $\psi_0^{(s)}$ with $\psi_0^{(a)}$ explains the northward displacement of the core of the zeroth-order solution. The current $\underline{u}_0^{(s)}$, having the same intensity along both zonal boundaries, is amplified in the northern region and reduced in the southern through the superposition with the cyclone–anticyclone couple given by $\psi_0^{(a)}$. Note that, a priori, the superposition of the cyclone with the anticyclonic circulation in the southern part of the basin ($0 \leq y \leq 1/2$) does not ensure the anticyclonic circulation of the resulting flow. However, if a counter-rotating pool of fluid would exist in a certain region R, of the subtropical basin, encircled by a streamline of ψ_0, then the lhs of Eq. (24) would be negative while the rhs would be positive. This contradiction prevents everywhere a zeroth-order cyclonic circulation.

5. Symmetric and antisymmetric components of the first-order correction

The symmetric and antisymmetric components of the first-order correction, ψ_{1s} and ψ_{1a}, are discussed in this section. They are used to explain the behavior of the residual streamfunction $\boldsymbol{D}$ (Fig. 1h and i and Fig. 2h and i), which approximates the first-order correction ψ_1 with an error of $O(\delta)$.

Using expansion (14) and substituting Eq. (15) into Eq. (5), we have

$$\epsilon^2[J(\psi_0, \nabla^2\psi_{1s}) + J(\psi_0, \nabla^2\psi_{1a}) + J(\psi_{1s}, \nabla^2\psi_0) + J(\psi_{1a}, \nabla^2\psi_0)] + \frac{\partial\psi_{1s}}{\partial x} + \frac{\partial\psi_{1a}}{\partial x} = T_s - \epsilon\nabla^2\psi_0. \tag{32}$$

By means of transform (11) applied to Eq. (32), we obtain the following equations for ψ_{1s} and ψ_{1a}:

$$\epsilon^2[J(\psi_0, \nabla^2\psi_{1a}) + J(\psi_{1a}, \nabla^2\psi_0)] + \frac{\partial\psi_{1a}}{\partial x} = T_s - \epsilon\nabla^2\psi_0 \tag{33}$$

and

$$\epsilon^2 J(\psi_0, \nabla^2\psi_{1s}) + J(\psi_{1s}, F(\psi_0)) = 0. \tag{34}$$

From Eq. (6), the boundary conditions are

$$\psi_{1a} = 0 \quad \text{along} \quad \partial D \tag{35}$$

and

$$\psi_{1s} = 0 \quad \text{along} \quad \partial D. \tag{36}$$

5.1. Antisymmetric component

Consider first problems (33) and (35). The presence of the cyclone–anticyclone couple in the first-order correction of Niiler's solution mentioned in the Section 1 is equivalent to the ascription, to the related streamfunction, of an antisymmetric component, in the sense of transform (11). To see that such kind of a flow pattern is not a peculiarity of that solution,

we verify by means of Eq. (31) that the hypothesis of vanishing ψ_{1a} through the fluid domain is incompatible with the typical wind-stress curl adopted in the models, besides that of Niiler ($T_s = 2y - 3$). If $\psi_{1a} \equiv 0$, then Eq. (33) implies the balance, point by point, $T_s(x, y) = \epsilon \nabla^2 \psi_0$ and hence, because of Eq. (17)

$$\epsilon T_s(x, y) + y = F(\psi_0). \tag{37}$$

We recall that, in general, $y = 0$ and $y = 1$ are the two consecutive latitudes such that $T_s(x, 0) = T_s(x, 1) = 0$, in the sense that this equation defines the latitudinal location of the gyre, rather than begin a constraint imposed on the wind-stress curl itself. Moreover, according to Eq. (4) $F(\psi_0) = F(0)\, \forall \underline{x} \in \partial D$, evaluation of Eq. (37) at $y = 0$ and $y = 1$ gives, respectively, $F(0) = 0$ and $F(0) = 1$. This inconsistency invalidates the hypothesis that $\psi_{1a} \equiv 0$. Note that, although the wind-stress curl does not vanish at $y = 0$ and $y = 1$ in Niiler's original model, Eq. (37) yields there, respectively, $-3\epsilon = 0$ and $-\epsilon + 1 = 0$, so that the same inconsistency holds also in that case.

We are led to conclude that in general $\psi_{1a} \neq 0$ through the fluid domain.

5.2. Symmetric component

Problem (34) subject (36) gives the symmetric part of the first-order correction. Few properties can be deduced analytically:

1. The possible nonvanishing solution has a zonal interior, whose isolines coincide with those of ψ_0 (in fact, disregarding the ϵ^2 term, Eq. (34) implies $\underline{\nabla}\psi_{1s} \times \underline{\nabla}\psi_0 = 0$);
2. The identically vanishing field

$$\psi_{1s} \equiv 0 \tag{38}$$

is an admissible solution because of the linearity of Eq. (34) and the homogeneity of Eq. (36).

Since the system (1) subject (2) on the whole prefers Eq. (38) rather than the nonvanishing solution coming from Eqs. (34) and (36), which we will obtain in the following, the question then arises about the ground of such a preference. In order to address this question, we consider the dissipation integral (24) which means that the circulation produced by the wind-stress on ∂R must be balanced by the dissipation of vorticity by bottom friction. However, balance (24) does not involve the total circulation but only its zeroth-order component. If the dissipation integral is extended to the whole domain, problems (1) and (2) state that, up to the first-order in δ,

$$\int_D T_s \, \mathrm{d}\underline{x} = \epsilon \left(\int_D \nabla^2 \psi_{0s} \, \mathrm{d}\underline{x} + \delta \int_D \nabla^2 \psi_1 \, \mathrm{d}\underline{x} \right). \tag{39}$$

Comparison to Eq. (24) evaluated in $R = D$ shows in Eq. (39) the survival of a dissipative term proportional to $\int_D \nabla^2 \psi_1 \, \mathrm{d}\underline{x}$. As steady circulation is impossible if the vorticity input is not exactly balanced by bottom dissipation, and this is yet realized by Eq. (24) with $R = D$, the circulation arranges itself in the basin to neutralize the surplus of dissipation coming from $\int_D \nabla^2 \psi_1 \, \mathrm{d}\underline{x}$. In other words, the first-order correction must satisfy the constraint

$$\int_D \nabla^2 \psi_1 \, \mathrm{d}\underline{x} = 0. \tag{40}$$

This is automatically verified by the antisymmetric part of ψ_1, whatever ψ_1 may be. In fact, setting $\chi_a = \nabla^2\psi_{1a}$ in Eq. (16), we have $\int_D \nabla^2\psi_{1a}\,d\underline{x} = 0$. On the other hand, the nonvanishing solutions of Eqs. (34) and (36) are not consistent with Eq. (40). On the other hand, the nonvanishing solutions of Eqs. (34) and (36) are not automatically consistent with Eq. (40), and as we demonstrate below by the use of boundary layer methods, are not, in fact, permitted at all. The remaining possibility is therefore given by Eq. (38), in accordance with the result obtained through the numerical integration of the starting problems (1) and (2) (Figs. 1i and 2i). We also point that the systems (1) and (2) appear to have a unique solution according to the study by Ierley and Sheremet (1995) that investigates the existence of multiple solutions of the barotropic quasigeostrophic equation subject to forcing, dissipation and domain configuration similar to those in the present study.

Problems (34) and (36), under the additional constraint,

$$\int_D \nabla^2\psi_{1s}\,d\underline{x} = 0, \tag{41}$$

admits, within the validity of the boundary layer approximation, only the identically vanishing solution (38).

We note, preliminarily, that Eq. (34) is equivalent to

$$\epsilon^2\,\nabla^2\psi_{1s} - \frac{\partial F}{\partial\psi_0}\,\psi_{1s} = G(\psi_0) \tag{42}$$

where G is any differentiable function of ψ_0. Then, because of Eqs. (4) and (36), Eq. (42) implies

$$\nabla^2\psi_{1s} = \frac{G(0)}{\epsilon^2} \quad \forall\underline{x} \in \partial D. \tag{43}$$

Eq. (43) will be useful in the following. Consider now Eq. (34) written as

$$\epsilon^2\,\underline{k}\cdot\underline{\nabla}\,\psi_0 \times \underline{\nabla}\,(\nabla^2\psi_{1s}) - \frac{\partial F}{\partial\psi_0}\,\underline{k}\cdot\underline{\nabla}\,\psi_0 \times \underline{\nabla}\,\psi_{1s} = 0 \tag{44}$$

and focus attention to the western boundary. We introduce the western boundary layer coordinate

$$\xi = \frac{L}{\ell}\,x \tag{45}$$

and define the boundary layer nondimensional width ℓ/L through the equation

$$\epsilon^2\left(\frac{L}{\ell}\right)^2 = F_0' \tag{46}$$

where F_0' is the constant value that $\partial F/\partial\psi_0$ takes along ∂D. The value ascribed to ϵ and the scatter plots of Figs. 1e and 2e are consistent with the inequality

$$\frac{L}{\ell} \gg 1. \tag{47}$$

According to the standard technique, we set

$$\psi_{\mathrm{W}} = \psi_{\mathrm{I}}(y) + \phi_{\mathrm{W}}(\xi, y) \tag{48}$$

where the zonality of the interior of $\psi_{1\mathrm{s}}$ immediately comes from the zonality of ψ_0 and the equation $J(\psi_0, \psi_{1\mathrm{s}}) = 0$ that holds in the interior (as it is the approximate version of Eq. (34) obtained by disregarding the term proportional to ϵ^2 at the basin scale).

From Eq. (48) we have, recalling Eq. (45),

$$\underline{\nabla}\,\psi_{\mathrm{W}} = \underline{\nabla}\,\psi_{\mathrm{I}} + \frac{L}{\ell}\,\frac{\partial \phi_{\mathrm{W}}}{\partial \xi}\underline{i} + \frac{\partial \phi_{\mathrm{W}}}{\partial y}\underline{j}$$

and, because of Eq. (7), the basic approximation

$$\underline{\nabla}\,\psi_{\mathrm{W}} \approx \frac{L}{\ell}\,\frac{\partial \phi_{\mathrm{W}}}{\partial \xi}\underline{i} \tag{49}$$

follows. Moreover, from Eq. (49), we easily evaluate

$$\nabla^2\,\psi_{1\mathrm{s}} \approx \left(\frac{L}{\ell}\right)^2\,\frac{\partial^2 \phi_{\mathrm{W}}}{\partial \xi^2} \tag{50}$$

and hence

$$\underline{\nabla}(\nabla^2 \psi_{1\mathrm{s}}) \approx \left(\frac{L}{\ell}\right)^3\,\frac{\partial^3 \phi_{\mathrm{W}}}{\partial \xi^3}\underline{i}. \tag{51}$$

Substitution of Eqs. (49), (50) and (51), into Eq. (44) and recalling also Eq. (46) give

$$\frac{\partial^3 \phi_{\mathrm{W}}}{\partial \xi^3} - \frac{\partial \phi_{\mathrm{W}}}{\partial \xi} = 0. \tag{52}$$

Eq. (52) must be supplemented by the conditions

$$\phi_{\mathrm{W}}(+\infty, y) = 0 \tag{53}$$

and

$$\psi_{\mathrm{I}}(y) + \phi_{\mathrm{W}}(0, y) = 0. \tag{54}$$

The unique solution of the problems (52)–(54) is

$$\phi_{\mathrm{W}} = -\psi_{\mathrm{I}}(y)\exp(-\xi) \tag{55}$$

and hence

$$\phi_{\mathrm{W}} = \psi_{\mathrm{I}}(y)\,[1 - \exp(-\xi)]. \tag{56}$$

Application of Eq. (43) to Eq. (56) gives

$$\nabla^2 \psi_{\mathrm{W}}|_{x=0} \approx -\psi_{\mathrm{I}}(y)\left(\frac{L}{\ell}\right)^2$$

and therefore, by resorting again to Eq. (46), we obtain

$$\psi_{\mathrm{I}}(y) = -\frac{G(0)}{F_0'}, \tag{57}$$

so

$$\psi_{\mathrm{W}} = -\frac{G(0)}{F_0'}\,[1 - \exp(-\xi)]. \tag{58}$$

In particular, the meridional current along the western boundary is

$$v(0, y) = \left.\frac{\partial \psi_{\mathrm{W}}}{\partial x}\right|_{x=0} = -\frac{L}{\ell}\,\frac{G(0)}{F_0'} = -\frac{G(0)}{\epsilon\sqrt{F_0'}}. \tag{59}$$

By repeating these calculations for the remaining sides of the boundary, we obtain, analogously to Eq. (59),

$$v(1, y) = \frac{G(0)}{\epsilon\sqrt{F_0'}}, \qquad u(x, 1) = -\frac{G(0)}{\epsilon\sqrt{F_0'}}, \qquad u(x, 0) = \frac{G(0)}{\epsilon\sqrt{F_0'}}. \tag{60}$$

The integral (41) can be written as

$$\int_0^1 [v(1, y) - v(0, y)]\,\mathrm{d}y - \int_0^1 [u(x, 1) - u(x, 0)]\,\mathrm{d}x = 0 \tag{61}$$

and the substitution of Eqs. (59) and (60) into Eq. (61) yields $4\,G(0)/\epsilon\sqrt{F_0'} = 0$, that is to say

$$G(0) = 0. \tag{62}$$

Eq. (62) implies through Eq. (58) that $\psi_{\mathrm{W}} = 0$, and in the same way, also $\psi_{\mathrm{N}} = \psi_{\mathrm{S}} = \psi_{\mathrm{E}} = 0$. This means that, within the boundary layer approximation, Eq. (38) follows.

The boundary layer method, which is characterized in the present context by Eq. (49), singles out a class of approximate solutions, each depending on a special value of $G(0)$. Within this class, constraint (41) implies Eq. (38). This result is consistent with the numerical experiments but, most likely, it is not exhaustive with respect to all the solutions of problems (34) and (36).

To summarize, $\psi_1 = \psi_{1\mathrm{a}}$ that states the overall antisymmetric structure of the first-order correction under transform (11).

6. Qualitative reconstruction of the weak westward intensification of a highly inertial subtropical gyre

The numerical solutions and analytical investigation presented in the previous sections have indicated that

$$\psi = \psi_{0\mathrm{s}} + \delta\,\psi_{1\mathrm{a}} + \mathrm{O}(\delta^2) \tag{63}$$

where $\psi_{0s} = \psi_0^{(s)} + \psi_0^{(a)}$ with both $\psi_0^{(s)}$ and $\psi_0^{(a)}$ nonvanishing. We recall that, if R is any region of the fluid domain encircled by a (closed) streamline of ψ_{0s}, Eq. (24) holds, that is $\int_R T_s \, d\underline{x} = \epsilon \oint_{\partial R} \underline{u}_0 \cdot d\underline{t}$, where $\underline{u}_0 = \underline{k} \times \underline{\nabla}\psi_{0s}$ is the zeroth-order geostrophic current. As the lhs of Eq. (24) is negative on all R and $d\underline{t}$ is positive anticlockwise, this component of the geostrophic current is clockwise along every streamline. In particular, along the eastern boundary the meridional velocity v_0 is southward while along the western boundary v_0 is northward. In accordance with Eq. (19), v_0 is antisymmetric

$$v_0 \equiv v_{0a} = \frac{\partial \psi_{0s}}{\partial x}.$$

On the contrary, the component of the meridional velocity relative to ψ_{1a}, that is

$$v_{1s} = \frac{\partial \psi_{1a}}{\partial x}$$

is symmetric and, therefore, it has the same direction along the meridional coasts. On the whole, $v = v_{0a} + \delta\, v_{1s}$, and v_{1s} is parallel to v_{0a} along one side but antiparallel along the other one. To understand why the $O(\delta)$ intensification takes place exactly in the west, consider the first-order velocity in the basin interior, where Eq. (33) simplifies to

$$\frac{\partial \psi_{1a}}{\partial x} \approx T_s \tag{64}$$

thus showing that there

$$v_{1s} \leq 0. \tag{65}$$

The inequality (65) together with the symmetry of v_1 implies that the return flows, demanded by mass conservation, must be northward. Therefore, we can write

$$v(x \approx 0) = |v_{0a}| + \delta\, |v_{1s}| \quad \text{while} \quad v(x \approx 1) = -|v_{0a}| + \delta\, |v_{1s}| \tag{66}$$

and the east–west asymmetry exhibited in Figs. 1a and 2a is explained. This result is reminiscent of that of Zimmerman (1993) reported in Fig. 1 of that paper, however, we point out that a constant wind-stress curl and a circular basin have been used in that study.

The weak westward intensification described by Eq. (66) together with the northward displacement of ψ_{0s}, discussed in Section 4, explains the tendency of the subtropical gyre to be centered in the northwestern area of the basin. We wish to underline that in the regime under investigation, $\delta \ll 1$ with $\epsilon < \delta$, the northward displacement and the weak westward intensification of the gyre are simultaneously and necessarily present. This is unlike both the linear case (e.g. Stommel, 1948) where the solution exhibits a strong westward intensification but it is exactly invariant for north–south exchange, and the fully inertial case (e.g. Fofonoff, 1954) where the solution has a gyre center markedly displaced northward, but is symmetric under east–west exchange.

A final comment about Eq. (64) is that in the frictional regime, the extension of a hypothetical ψ_{1a} up to the eastern boundary would be achieved by solving the problem

$$\frac{\partial \psi_{1a}}{\partial x} = T_s \quad \text{and} \quad \psi_{1a}(1, y) = 0$$

whose solution is

$$\psi_{1a}(x, y) = -\int_x^1 T_s(\lambda, y)\, d\lambda. \tag{67}$$

However, it is easy to check that $-\psi_{1a}(1-x, y) = \int_0^x T_s(\lambda, y)\, d\lambda$ and this last function does not coincide with Eq. (67), so ψ_{1a} is no longer antisymmetric. In other words, the symmetry properties that are introduced by high nonlinearity extend to the whole basin, thus preventing us from finding purely local solutions, by using, e.g. boundary layer methods in weakly nonlinear models.

As the final note, we consider the basin-integrated energy balance, obtained by multiplying Eq. (1) by ψ and integrating each product on D with the aid of Eq. (2):

$$\int_D \psi_{0s}\, T_s\, d\underline{x} + \delta \int_D \psi_{1a}\, T_s\, d\underline{x} + \epsilon \int_D |\underline{\nabla}\psi_{0s}|^2\, d\underline{x} + 2\epsilon\delta \int_D |\underline{\nabla}\psi_{0s}| \cdot \underline{\nabla}\psi_{1a}\, d\underline{x}.$$

As $\psi_{1a}\, T_s$ and $\underline{\nabla}\psi_{0s} \cdot \underline{\nabla}\psi_{1a}$ are antisymmetric functions, the related integrals are separately zero and the last equation reduces to

$$\int_D \psi_{0s}\, T_s\, d\underline{x} = -\epsilon \int_D |\underline{\nabla}\psi_{0s}|^2\, d\underline{x}. \tag{68}$$

According to Eq. (68),

$$\int_D \psi_{0s}\, T_s\, d\underline{x} < 0, \tag{69}$$

i.e. by resorting to the stress $\underline{\tau}$ and the zeroth-order velocity $\underline{u}_0$ we can also write

$$\int_D \underline{u}_0 \cdot \underline{\tau}\, d\underline{x} > 0. \tag{70}$$

The inequality (70) means that the wind does work on the zeroth-order flow, while, because of the symmetry properties of ψ_1, $\int_D \underline{u}_1 \cdot \underline{\tau}\, d\underline{x} \equiv 0$. Griffa and Salmon (1989) have shown numerically, in the framework of the equilibrium statistical mechanics applied to the barotropic quasi-geostrophic dynamics that if Eq. (70) holds, then, when the wind-stress and bottom drag are switched on ($\delta \to 0$ in our notation), the nonlinear terms still try to drive the flow towards the Fofonoff flow. They state also that Niiler's model applies only to winds that can do positive work on Fofonoff's flow, that is just our inequality (69). Finally, we recall that all the experiments of Griffa and Salmon (1989) were performed by using symmetric forcing of the kind $T_s = T_s(y)$.

7. Summary and conclusions

In this paper, we explore symmetry properties of steady solutions of the quasi-geostrophic version of Niiler's (1966) model (Crisciani, 1998) in an intermediate regime, where both inertial and beta terms are important. The system that is considered consists of a barotropic single gyre, subject to an anticyclonic wind forcing and bottom friction. The analytical

investigation is conducted by perturbing the fully inertial solution (zeroth-order solution) via the forcing and dissipation (leading to the first-order correction). The numerical solutions supported by analytical arguments demonstrate that the full solution can be approximated as the sum of three components: $\psi \approx \psi_0^{(s)} + \psi_0^{(a)} + \delta\psi_{1a}$, i.e. the sum of the north–south symmetric and antisymmetric components of the zeroth-order solution and the east–west antisymmetric component of the first-order correction. The original aspect of this study is the perspective brought by considering the symmetry properties of these components. In the regime of interest, defined by $\delta \ll 1$ with $\epsilon < \delta$, the center of the gyre tends to be in the northwest corner of the domain. The observed asymmetry of the total solution is then explained by being due to the north–south asymmetry of the zeroth-order solution and the east–west antisymmetry of the first-order correction. The flow patterns of the individual components are discussed and the symmetry properties of these partial solutions are linked to the integral vorticity balance of the system. The analytical considerations and numerical experiments are repeated for two kinds of single-gyre wind-forcing patterns and the results indicate that the general conclusions discussed above are to some extent independent of the details of the wind forcing.

Finally, we point out the limitation of our results in the sense that while they appear to be valid in the context of the classical, bottom-dissipated, single-gyre in a square ocean basin, the general derivation of symmetry properties for a class of basins and a class of forcings is a far more demanding task, and will be pursued in a future study.

Acknowledgements

F. Crisciani wishes to thank Roberto Purini for useful discussions and acknowledges partial support from ASI (Italian Space Agency). T.M. Özgökmen acknowledges the support of the National Science Foundation grant OCE 9711186. Both authors greatly appreciate the comments and suggestions of J. Pedlosky. Finally, the authors thank the two anonymous reviewers, whose detailed comments have improved the manuscript.

References

Arakawa, A., 1966. Computational design for long-term numerical integration of the equations of fluid motion: two dimensional incompressible flow. Part I. J. Comput. Phys. 1, 119–143.

Crisciani, F., 1998. Stability of Niiler's solution of the general circulation problem. J. Phys. Oceanogr. 28, 218–226.

Crisciani, F., Purini, R., 1997. Boundary condition of the Sverdrup solution from flow energetics. J. Phys. Oceanogr. 27, 357–361.

Fofonoff, N.P., 1954. Steady flow in a frictionless homogeneous ocean. J. Mar. Res. 13, 254–262.

Gazdag, J., 1976. Time-differencing schemes and transform methods. J. Comput. Phys. 20, 196–207.

Griffa, A., Salmon, R., 1989. Wind-driven ocean circulation and equilibrium mechanics. J. Mar. Res. 47, 457–492.

Ierley, G.R., Sheremet, V.A., 1995. Multiple solutions and advection-dominated flows in the wind-driven circulation. Part I: Slip. J. Mar. Res. 53, 703–737.

Niiler, P.P., 1966. On the theory of wind-driven circulation. Deep-Sea Res. 13, 597–606.

Pedlosky, J., 1965. A note on the western intensification of the oceanic circulation. J. Mar. Res. 23, 207–209.

Stommel, H., 1948. The westward intensification of wind-driven currents. Trans. Am. Geophys. Union 19, 202–206.

Swarztrauber, P.N., 1977. The methods of cyclic reduction, Fourier analysis and FACR algorithm for discrete solution of the Poisson equation on a rectangle. SIAM Rev. 19, 490–501.

Veronis, G., 1966. Wind-driven circulation Part II. Deep-Sea Res. 13, 30–55.

Zimmerman, J.T.F., 1993. A simple model for the symmetry properties of non-linear wind driven ocean circulation. Astrophys. Fluid Dynamics 71, 1–15.

Zimmerman, J.T.F., Maas, L.R.M., 1989. Renormalized Green's function for nonlinear circulation on the beta plane. Phys. Rev. A 39 (7), 3575–3590.